A modeling to understand where a vertical crack can propagate in pavements

Armelle Chabot, Quang Dat Tran, Alain Ehrlacher

A modeling to understand where a vertical crack can propagate in pavements

A. Chabot
Division Matériaux et Structures de Chaussées - LCPC, Bouguenais, France

Q. D. Tran
Laboratoire Analyse et identification des Matériaux – NPC, Marne la Vallée, France

A. Ehrlacher
Laboratoire Analyse et identification des Matériaux – NPC, Marne la Vallée, France

ABSTRACT: To understand how a pre-existing vertical crack can propagate and damage pavements an alternative modeling is proposed to be used. For the multilayered pavement structures, the simplified modelling, named the multi-particle model of multi-layer materials (M4) with 5n equilibrium equations (n: number of pavement layers) is linked to the Boussinesq solution for the soil (Tran, 2004) (Chabot et al., 2005). This approach has the advantage of reducing the real 3D problem to the determination of regular plane fields (x,y) per layer and interface. Heavy loads, thermal loadings and thermal shrinkage phenomena have been integrated and validated with respect to finite element computations. It shows that the bond between layers near vertical cracks is damaged by normal and shear stresses. These combined effects are proposed to be modeled to understand corner crack initiation phenomenon of cemented concrete slab. Surface observations on concrete pavements with joints help the discussion.

1 INTRODUCTION

In the aim of proposing durable structures and reducing the maintenance costs incurred on French highways, it is highly necessary to fully comprehend and model the various pavement failure mechanisms that often stem from the presence of cracks. Classical semi-analytical model makes it possible to compute an elastic multilayer lying on a semi-infinite solid submitted to circular loading; however, incorporating the viscoelastic characteristic of asphalt layers (Duhamel et al., 2005), their damage (Bodin et al., 2004) or the nature of cracks (Tran et al., 2004) requires major developmental breakthroughs beyond the typical design methods.

As pavements are composed by superimposing layers of different materials with different elastic properties, it is well known that stress singularities appear at the interface on the free edges generated by vertical cracks (Fig. 1).

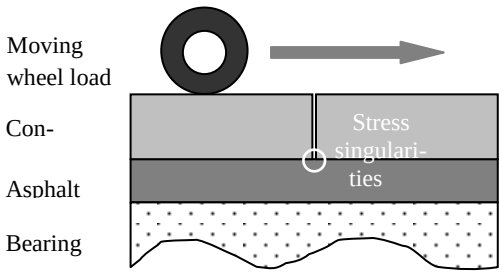

Figure 1. Example of stress singularities at the interface near a crack on a loaded composite pavement structure (Pouteau et al., 2004)

The modeling of cracked 3D pavement structures by means of finite elements is indeed possible (Romanoschi and Li, 2002). Yet the level of mesh refinement near cracks required to obtain significant results makes the method quite costly in terms of computation time and due to stress singularities special methods have to be found to analyze correctly the results. In order to produce a diagnostic and maintenance software that performs computations quickly and efficiently for use on worn pavements, a dedicated model has been developed at both ENPC and LCPC (Tran, 2004) (Tran et al., 2004) (Chabot et al., 2005). It is proposed here to fully present it for the mechanical understanding of corner cracks phenomenon in cemented concrete slabs.

2 THE MODELLING

To summarize, this paragraph contains only the main equations of the modelling. The interested reader can refer to Tran's doctoral thesis (2004) for a complete model description.

In the following purpose, (x,y,z) will denote the three coordinates of a point in the reference system (O,ex,ey,ez). The indices of plane tensor components is denoted by Greek letters (e.g. plane components of the stress tensor are written as $\sigma_{\alpha\beta}$).The n layers of the multilayer assembly are stacked along the downward-oriented direction of the ez axis of this coordinate system. Index i designates the layer number within the sequence {1, ..., n}. The double index i, i + 1 indicates the interface between layers i and i + 1 (see Figure 4).

The layer i is composed of the set of points (x,y,z), such that: $z \in \left[h_i^-, h_i^+\right] \quad \left(h_{i+1}^- = h_i^+\right)$. $e^i = h_i^+ - h_i^-$ represents layer thickness and $\bar{h}^i = \left(h_i^+ + h_i^-\right)/2$ its average dimension on the e3 axis. Pavement layers i are chosen to be isotropic linear elastic, with Young's modulus E_i and Poisson's ratio υ_i. The soil is elastic, linear and isotropic, characterized by its Young's modulus E_s and Poisson's ratio υ_s.

2.1 *Multiparticle model of multilayered materials with 5n equilibrium equations (designated M4-5n) for pavement layers*

The multiparticle model of multilayered materials (M4) adopted for this bending problem comprises five kinematic fields for each layer i (i = 1, ..., n) (5n); this model makes up part of the M4 family developed at the Ecole Nationale des Ponts et Chaussées to study, in elasticity (Chabot, 1997) and (Chabot and Ehrlacher, 1998) then in inelasticity (Diaz Diaz et al. 2002), edge effects for composite structures.

Let's denote $u_j(x,y,z)$ (with j = 1,3) the 3D displacement fields, the kinematics of associated layers i (i = 1, ..., n) then contain the following average in-plane and out-of-plane displacements:

$$U_\alpha^i(x,y) = \int_{h_i^-}^{h_i^+} \frac{1}{e^i} u_\alpha(x,y,z)dz \text{ and } U_3^i(x,y) = \int_{h_i^-}^{h_i^+} \frac{1}{e^i} u_3(x,y,z)dz \qquad (1)$$

along with the average rotations defined as follows:

$$\Phi_\alpha^i(x,y) = \int_{h_i^-}^{h_i^+} \frac{12\left(z-\bar{h}^i\right)}{{e^i}^3} u_\alpha(x,y,z)dz \qquad (2)$$

The M4-5n may be considered like superimposing n Reissner plates. Its construction relies on a 1st-degree polynomial approximation of the membrane stress fields in z. The expression of 3D equilibrium equations yields 2nd- and 3rd-degree polynomials in z per layer for shear stresses and normal stress, respectively. The coefficients of these polynomials for each layer are correlated with the classical generalized force and moment fields of Reissner plates. Such ap-

proximations offer the advantage of defining at the $i,i+1$ interfaces both the shear stresses $\tau_\alpha^{i,i+1}(x,y)$ and normal stresses $\nu^{i,i+1}(x,y)$ such that: $\tau_\alpha^{i,i+1}(x,y)=\sigma_{\alpha 3}\left(x,y,h_i^+\right)=\sigma_{\alpha 3}\left(x,y,h_{i+1}^-\right)$ and $\nu^{i,i+1}(x,y)=\sigma_{33}\left(x,y,h_i^+\right)=\sigma_{33}\left(x,y,h_{i+1}^-\right)$.

The Hellinger-Reissner function is used to obtain the equations expressed in generalized variables. The actual 3D multilayered problem can then be reduced to determining fields in (x,y) for each layer i and each interface between layers i, i + 1, thus transforming the real 3D object into a 2D geometric object. Furthermore, the M4 model diverts focus from edge effects, resulting in a finite value of stresses at plate edges. Between two adjacent material layers, it then becomes possible to express delamination criteria in terms of interfacial forces (Chabot et al., 2000) (Caron et al., 2006). On finite structures, the M4-5n fields are very close to those obtained from a refined approach involving 3D finite elements (Carreira et al., 2002).

In sum, after combining the various M4-5n equilibrium and constitutive equations, a system of five 2nd-order differential equations for each layer i of the pavement multilayer (i = 1, ..., n) in the (x,y) plane can be generated. The system has been presented below under the hypothesis that volume forces are negligible.

$$e_iE_i\left(\frac{1}{1-\upsilon_i^2}U_{1,11}^i+\frac{1}{2\left(1+\upsilon_i\right)}U_{1,22}^i+\frac{1}{2\left(1-\upsilon_i\right)}U_{2,12}^i\right)=\tau_1^{i-1,i}-\tau_1^{i,i+1}+\frac{e^iE^i}{\left(1-\upsilon_i^2\right)}\left(\varepsilon_{11}^{i\ in}+\upsilon_i\,\varepsilon_{22}^{i\ in}\right)_{,1}+\frac{e^iE^i}{\left(1+\upsilon_i\right)}\varepsilon_{12}^{i\ in}{}_{,2} \tag{3}$$

$$e_iE_i\left(\frac{1}{2\left(1+\upsilon_i\right)}U_{2,11}^i+\frac{1}{1-\upsilon_i^2}U_{2,22}^i+\frac{1}{2\left(1-\upsilon_i\right)}U_{1,12}^i\right)=\tau_2^{i-1,i}-\tau_2^{i,i+1}+\frac{e^iE^i}{\left(1-\upsilon_i^2\right)}\left(\upsilon_i\,\varepsilon_{11}^{i\ in}+\varepsilon_{22}^{i\ in}\right)_{,2}+\frac{e^iE^i}{\left(1+\upsilon_i\right)}\varepsilon_{12}^{i\ in}{}_{,1} \tag{4}$$

$$\frac{2e_i^2E_i}{1-\upsilon_i^2}\Phi_{1,11}^i+\frac{e_i^2E_i}{1+\upsilon_i}\Phi_{1,22}^i+\frac{e_i^2E_i}{1-\upsilon_i}\Phi_{2,12}^i-\frac{10E_i}{1+\upsilon_i}\left(U_{3,1}^i+\Phi_1^i\right)=-10\left(\tau_1^{i-1,i}+\tau_1^{i,i+1}\right)+\frac{e^{i\,3}E^i}{\left(1-\upsilon_i^2\right)}\left(\chi_{11}^{i\ in}+\upsilon_i\,\chi_{22}^{i\ in}\right)_{,1}+\frac{e^{i\,3}E^i}{\left(1+\upsilon_i\right)}\chi_{12,2}^{i\ in} \tag{5}$$

$$\frac{e_i^2E_i}{1+\upsilon_i}\Phi_{2,11}^i+\frac{2e_i^2E_i}{1-\upsilon_i^2}\Phi_{2,22}^i+\frac{e_i^2E_i}{1-\upsilon_i}\Phi_{1,12}^i-\frac{10E_i}{1+\upsilon_i}\left(U_{3,2}^i+\Phi_2^i\right)=-10\left(\tau_2^{i-1,i}+\tau_2^{i,i+1}\right)+\frac{e^{i\,3}E^i}{\left(1-\upsilon_i^2\right)}\left(\upsilon_i\,\chi_{11}^{i\ in}+\chi_{22}^{i\ in}\right)_{,2}+\frac{e^{i\,3}E^i}{\left(1+\upsilon_i\right)}\chi_{12,1}^{i\ in} \tag{6}$$

$$U_{3,11}^i+U_{3,22}^i+\Phi_{1,1}^i+\Phi_{2,2}^i=\frac{12\left(1+\upsilon_i\right)}{5e_iG_i}\left(\nu^{i-1,i}-\nu^{i,i+1}\right)-\frac{\left(1+\upsilon_i\right)}{5E_i}\left(\tau_{1,1}^{i,i+1}+\tau_{2,2}^{i,i+1}+\tau_{1,1}^{i-1,i}+\tau_{2,2}^{i-1,i}\right)+d_{\Phi 1,1}^{i\ in}+d_{\Phi 2,2}^{i\ in} \tag{7}$$

$\varepsilon_{\alpha\beta}^{i\ in}(x,y)$, $\chi_{\alpha\beta}^{i\ in}(x,y)$ and $d_{\Phi\alpha}^{i\ in}(x,y)$ denote respectively inelastic in plane strains, inelastic in plane curvatures and inelastic shear strains of the layer i . $D_\alpha^{i,i+1\ in}(x,y)$, and $D_3^{i,i+1\ in}(x,y)$ are respectively the in plane and out of plane displacement discontinuities at the interface i,i+1. These fields are supposed to be known.

Similarly, a system of three 1st-order differential equations per interface $i,i+1$ $(i=1,...,n-1)$ is obtained as follows:

$$U_1^{i+1}-U_1^i-\frac{5e_i}{12}\Phi_1^i-\frac{5e_{i+1}}{12}\Phi_1^{i+1}+\frac{e_i}{12}U_{3,1}^i+\frac{e_{i+1}}{12}U_{3,1}^{i+1}-D_1^{i,i+1\,in}=-\frac{e_i(1+\upsilon_i)}{12E_i}\tau_1^{i-1,i}$$
$$+\frac{1}{8}\left(\frac{2e_i(1+\upsilon_i)}{E_i}+\frac{2e_{i+1}(1+\upsilon_{i+1})}{E_{i+1}}\right)\tau_1^{i,i+1}-\frac{e_{i+1}(1+\upsilon_{i+1})}{12E_{i+1}}\tau_1^{i+1,i+2} \quad (8)$$

$$U_2^{i+1}-U_2^i-\frac{5e_i}{12}\Phi_2^i-\frac{5e_{i+1}}{12}\Phi_2^{i+1}-\frac{e_i}{12}U_{3,2}^i-\frac{e_{i+1}}{12}U_{3,2}^{i+1}-D_2^{i,i+1\,in}=-\frac{e_i(1+\upsilon_i)}{12E_i}\tau_2^{i-1,i}$$
$$+\frac{1}{8}\left(\frac{2e_i(1+\upsilon_i)}{E_i}+\frac{2e_{i+1}(1+\upsilon_{i+1})}{E_{i+1}}\right)\tau_2^{i,i+1}-\frac{e_{i+1}(1+\upsilon_{i+1})}{12E_{i+1}}\tau_2^{i+1,i+2} \quad (9)$$

$$U_3^{i+1}-U_3^i-D_3^{i,i+1\,in}=\frac{9e_i}{70E_i}\nu^{i-1,i}+\frac{13}{35}\left(\frac{e_i}{E_i}+\frac{e_{i+1}}{E_{i+1}}\right)\nu^{i,i+1}+\frac{9e_{i+1}}{70E_{i+1}}\nu^{i+1,i+2} \quad (10)$$

Forces at the n, n+1 interface between the last layer n at the bottom of the pavement multi-layer and the ground are the unknowns to be found. They depend on the interaction (whether bonded or not) between ground and the pavement structure (Fig. 4).

2.2 *Boussinesq equations for the soil mass*

For building high-speed computation software, the analytical solution of the Boussinesq model stands out as the most viable for the modelling of the semi-infinite elastic soil mass.

The overlap of the two models proceeds by either the continuity or non-continuity of displacement fields at the $n,n+1$ interface of the n pavement layers and the ground (Fig. 4). Three additional equations yield the relation between surface displacements $u_j^{surface}(x,y)\quad(j\in\{1,2,3\})$ of the Boussinesq soil mass and M4-5n interfacial stresses $\tau_\alpha^{n,n+1}(x,y)$ and $\nu^{n,n+1}(x,y)$ as presented below for the bonded case.

$$u_1^{surface}(x,y)=U_1^n(x,y)+\frac{e^n}{2}\Phi_1^n(x,y)$$
$$=\frac{(1+\upsilon_s)}{\pi E_s}\times\begin{pmatrix}-\frac{1-2\upsilon_s}{2}\int_S\nu^{n,n+1}(\xi,\eta)\frac{(x-\xi)}{(x-\xi)^2+(y-\eta)^2}d\xi d\eta\\+\int_S\tau_1^{n,n+1}(\xi,\eta)\frac{(x-\xi)^2+(1-\upsilon_s)(y-\eta)^2}{\left((x-\xi)^2+(y-\eta)^2\right)^{3/2}}d\xi d\eta\\+\upsilon_s\int_S\tau_2^{n,n+1}(\xi,\eta)\frac{(x-\xi)(y-\eta)}{\left((x-\xi)^2+(y-\eta)^2\right)^{3/2}}d\xi d\eta\end{pmatrix} \quad (11)$$

$$u_2^{surface}(x,y)=U_2^n(x,y)+\frac{e^n}{2}\Phi_2^n(x,y)$$
$$=\frac{(1+\upsilon_s)}{\pi E_s}\times\begin{pmatrix}-\frac{1-2\upsilon_s}{2}\int_S\nu^{n,n+1}(\xi,\eta)\frac{(y-\eta)}{(x-\xi)^2+(y-\eta)^2}d\xi d\eta\\+\upsilon_s\int_S\tau_1^{n,n+1}(\xi,\eta)\frac{(x-\xi)(y-\eta)}{\left((x-\xi)^2+(y-\eta)^2\right)^{3/2}}d\xi d\eta\\+\int_S\tau_2^{n,n+1}(\xi,\eta)\frac{(1-\upsilon_s)(x-\xi)^2+(y-\eta)^2}{\left((x-\xi)^2+(y-\eta)^2\right)^{3/2}}d\xi d\eta\end{pmatrix} \quad (12)$$

$$u_3^{surface}(x,y) = U_3^n(x,y)$$
$$= \frac{(1+\upsilon_s)}{\pi E_s} \times \left(\begin{array}{l} (1-\upsilon_s)\int_S \nu^{n,n+1}(\xi,\eta) \frac{1}{\left((x-\xi)^2+(y-\eta)^2\right)^{1/2}} d\xi d\eta \\ + \frac{(1-2\upsilon_s)}{2} \left(\begin{array}{l} \int_S \tau_1^{n,n+1}(\xi,\eta) \frac{(x-\xi)}{(x-\xi)^2+(y-\eta)^2} d\xi d\eta \\ + \int_S \tau_2^{n,n+1}(\xi,\eta) \frac{(y-\eta)}{(x-\xi)^2+(y-\eta)^2} d\xi d\eta \end{array} \right) \end{array} \right) \quad (13)$$

In the following discussion, we will refer to the combination of the M4-5n model for pavement layers and the Boussinesq soil model as "M4-5nB". The Figure 4 shows its diagram.

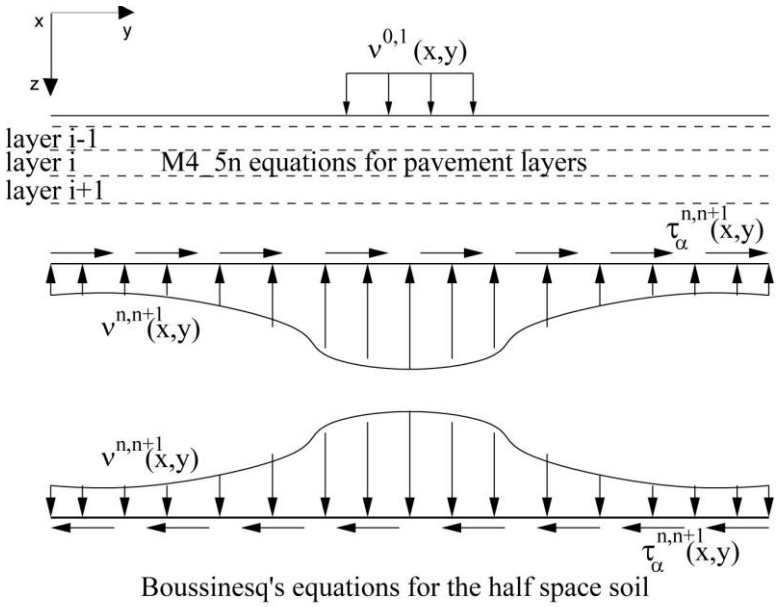

Figure 4. Diagram of the pavement modelling M4-5nB (Tran et al., 2004)

2.3 *M4-5nB boundary conditions*

Forces at the 0,1 interface between the exterior and the first pavement layer serve as the model givens; they are correlated with the set of presumed known loading conditions of a truck wheel rolling over the pavement (Fig. 4).

In order to express the various boundary condition systems of pavement multilayer edges (or cracks) as a function of both the kinematic unknowns and interface forces, the constitutive equations of layer i from M4-5n are used (Chabot, 1997). Introducing cracks that are either longitudinal or transverse with respect to traffic load direction, or vertical over the thickness of one or several layers, requires considering that crack lips constitute two free edges, whose distance interval from one another is assumed nonzero, yet still narrow (on the order of one to several millimeters, depending on the type of pavement under examination).

On the unloaded edges (or vertical cracks) of pavement layers i (i = 1, ..., n), free edge boundary conditions are imposed. In this case, they may be expressed in the form of the five equation-per-layer system. For purposes of illustration, they have been listed below for any y whenever x becomes infinite (or tends to a finite value in the case of a crack):

$$\lim_{x\to\pm\infty}\left(\left(U_{1,1}^{i}(x,y)+\upsilon_i U_{2,2}^{i}(x,y)\right)-\left(\varepsilon_{11}^{i\ in}(x,y)+\upsilon_i\varepsilon_{22}^{i\ in}(x,y)\right)\right)=0$$
$$\lim_{x\to\pm\infty}\left(\left(\Phi_{1,1}^{i}(x,y)+\upsilon_i\Phi_{2,2}^{i}(x,y)\right)-\left(\chi_{11}^{i\ in}(x,y)+\upsilon_i\chi_{22}^{i\ in}(x,y)\right)\right)=0$$
$$\lim_{x\to\pm\infty}\left(\left(U_{1,2}^{i}(x,y)+U_{2,1}^{i}(x,y)\right)-2\varepsilon_{12}^{i\ in}(x,y)\right)=0 \qquad (14)$$
$$\lim_{x\to\pm\infty}\left(\left(\Phi_{1,2}^{i}(x,y)+\Phi_{2,1}^{i}(x,y)\right)-2\chi_{12}^{i\ in}(x,y)\right)=0$$
$$\lim_{x\to\pm\infty}\left(\Phi_{1}^{i}(x,y)+U_{3,1}^{i}(x,y)+\frac{(1+\upsilon_i)}{5E_i}\left(\tau_1^{i-1,i}(x,y)+\tau_1^{i,i+1}(x,y)\right)\right)=0$$

On the blocked edges of pavement layers i (i = 1, ..., n), e.g. far from the loading where the material is confined, the boundary conditions are also expressed in the form of the five equation-per-layer system. Again for illustration, they have been displayed below for any y whenever x becomes infinite (or tends to a finite value):

$$\lim_{x\to\pm\infty}U_1^i(x,y)=0,\ \lim_{x\to\pm\infty}\Phi_1^i(x,y)=0$$
$$\lim_{x\to\pm\infty}\left(U_{1,2}^{i}(x,y)+U_{2,1}^{i}(x,y)\right)=0,\ \lim_{x\to\pm\infty}\left(\Phi_{1,2}^{i}(x,y)+\Phi_{2,1}^{i}(x,y)\right)=0 \qquad (15)$$
$$\lim_{x\to\pm\infty}\left(\Phi_{1}^{i}(x,y)+U_{3,1}^{i}(x,y)+\frac{(1+\upsilon_i)}{5E_i}\left(\tau_1^{i-1,i}(x,y)+\tau_1^{i,i+1}(x,y)\right)\right)=0$$

2.4 *Resolution of the M4-5nB model equations*

To write the overall system of M4-5nB equations, interface equations (8) to (10) are used to eliminate forces $\tau_1^{i,i+1},\tau_2^{i,i+1}$ *et* $\nu^{i,i+1}$ (i = 1, ..., n – 1) in M4-5n equations (3) through (7) (i = 1, ..., n) that get associated with equations (11) to (13) from Boussinesq's analytical model.

Ultimately, presentation of the initial 3D problem is reduced to solving a 2D problem laid out in the plane composed of 5n+3 equations with 5n+3 plane unknown fields. Once the loading boundary conditions, known at the pavement multilayer surface, have been applied, system generalization can be synthesized in the form a global 2nd-order, 5n-dimensional differential system. The system of the three linear equations complementary to Boussinesq's equations (11) (12) (13) is provided (Tran, 2004) (Chabot et al., 2005).

To numerically solve the 5n-differential system, the Newmark finite differences method is applied. The 2D plane is discretized into N intervals along the x-axis and M intervals along the y-axis. By combining Newmark equations and the pavement multilayer system, the 2nd-order derivatives then 1st-order derivatives with respect to x are eliminated. Operation is once again employed to eliminate derivatives with respect to y. The resultant linear system thus contains $5n(N-1)(M-1)$ equations. Generalized for n layers, the discretized expression of the five boundary conditions for each layer i may be written on each plane edge in the form of the following systems of 1st-order differential $5n\times 2NM$ remaining equations with $\tau_1^{0,1},\tau_2^{0,1},\nu^{0,1}$ being the stress loading boundary conditions.

To facilitate Boussinesq integration steps, which may be performed analytically, it is assumed in an initial approximation that the interface forces remain constant over all elementary surfaces of the discretized plane. By changing variables, the integral of functions can easily be computed analytically.

In the discretized diagram, the crack is numerically represented by a discontinuity between two lines of points marking the crack edges. For these crack lip point lines, crack introduction into the 5n-dimensionnal previous linear system of equations consists of deleting the corresponding equations and replacing them by boundary condition point lines of the free edge type given in previously-discretized systems of boundary conditions.

3 VALIDATION WORK

Depending on the specific case, M4-5nB computations have been compared with either the 2D axi-symmetric computation results from the French Alizé software built with the Burmister model and 3D finite element results from the CESAR-LCPC code (Tran, 2004).

As regards multilayered structures, many authors over the past 30+ years (particularly in the field of composite materials) have demonstrated that the presence of free edges or cracks, in conjunction with material behavior heterogeneity on both sides of interlayer interfaces, leads to significant out-of-plane stress concentrations at the interfaces. This phenomenon requires further study before structural failure can be effectively predicted. Thus, in the aim of lightening the presentation of computation validation results, it was decided to proceed by illustrating just those results determined on out-of-plane stress fields at the interfaces.

In the following, a shrinkage case validation compared with 3D FEM results is presented. Figure 5 displays validations of interface stresses between two layers of a semi-rigid pavement structure cracked vertically through its cemented concrete layer. The load is expressed in the form of a uniform pressure $q = 0.662MPa$ on a rectangular surface of length $2a = 0.30m$ (along the traffic direction) and width $2b = 0.22m$. The pavement is composed of 2 elastic layers ($e_1 = 0.1m$, $E_1 = 9300MPa$, $\upsilon_1 = 0.35$; $e_1 = 0.3m$, $E_2 = 23000MPa$, $\upsilon_2 = 0.25$) lying on top of the soil mass of the French PF2 type ($E_s = 50MPa, \upsilon_s = 0.35$). The 3D finite element mesh comprises a total of 1,965 20-node volume elements and 7,080 15-node elements. A 5-m transverse dimension ensures the sufficiency condition is being met to simulate only a quarter of the structure. The M4-5nB plane mesh only contains 24×32 links for the all structure. Blocked edge-type boundary conditions have been chosen for this procedure.

Due to shrinkage effects, the temperature in all the second layer is assumed to change in a uniform way ($\delta T = 10°C$) with a coefficient of expansion $\alpha = 1.2 10^{-6} C^{-1}$. On the edge of the vertical crack of the second layer, this condition gives values of inelastic fields as $\varepsilon_{11}^{2\ in} = \varepsilon_{22}^{2\ in} = \alpha\,\delta T$ and $D_3^{1,2\ in} = e_2\,\alpha\,\delta T$. All other inelastic fields $\varepsilon_{12}^{2\ in}$ $\chi_{\alpha\beta}^{2\ in}(x,y), d_{\Phi\alpha}^{2\ in}(x,y)$ $D_\alpha^{1,2\ in}(x,y)$ are zero (Tran, 2004).

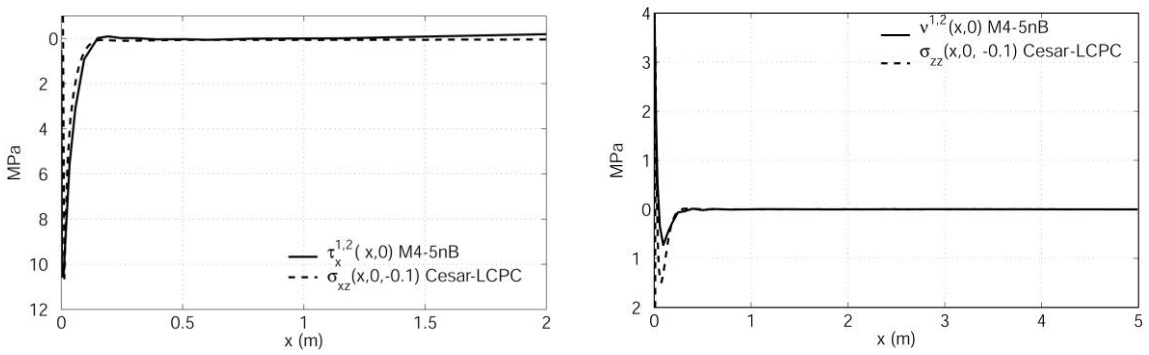

Figure 5. M4- 5nB interface stress fields validations for a shrinkage application case (Tran, 2004)

The computation of cracked pavement, assumed two-dimensional for this model set-up, reveals a very close approximation of stress fields at the various interfaces. For the interface 1,2 on Figure 5, the difference of stress intensity observed for the normal stress $v^{1,2}$ is due to 3D finite element results that become singular as the mesh becomes finer. The solution, programmed using Matlab software, is obtained by M4-5nB roughly 10 times faster than that derived from a finely-meshed 3D finite element computation near the crack. With shrinkage, thermal and loads effects, applying this vertical cracking configuration at the base of the dual pavement layer, is enabled analyzing stresses as part of research studies on the reinforcement of semi-rigid pavements or bottom-up cracking phenomenon.

4 RESULTS ON A COMPOSITE PAVEMENT APPLICATION

For the last ten years, new composite pavement structures have raised a significant interest. These are made of a concrete layer bonded on an asphalt sub-base. If the durability of this bond is proved, these structures benefit by a reduction both on the layers thickness and the cost (Pouteau, 2004) (Pouteau et al., 2004). However, the restrained shrinkage of the concrete layer leads to vertical cracks. To study the bond of composite pavement structures, an in-situ experiment has been performed using an accelerated pavement loading facility (Pouteau et al., 2006). With that so-called M4-Boussinesq model, it is proposed to analyze the initial mechanical fields of that in-situ experiment (Chabot et al., 2004).

The following section will present, for illustration purposes, an initial elastic approximation of these results via the M4-5nB model programmed in its "Research" version and run using the Matlab tool (Tran, 2004) (Guillo, 2004), in the case of blocked edges.

Being in the linear elastic mode, we can superimpose various loading cases. Thus to determine the interface stress state, it is only necessary to study the case where the load is at the edge of the crack. The load is considered rectangular ($2a = 0.28m$ and $2b = 0.18m$) with a uniform pressure $q = 0.645MPa$ while the pavement is considered to be composed of two elastic layers 1.95 m wide (French category 5 cement concrete: $e_1 = 0.08m$, $E_1 = 36500MPa$, $\upsilon_1 = 0.25$; asphalt overlay of the French GB3 type: $e_2 = 0.095m$, $E_2 = 8485MPa$ et $\upsilon_2 = 0.35$) on top of the soil mass (infinite within the plane) of the French PF3 type: $E_s = 120MPa$, $\upsilon_s = 0.35$. The M4-5nB plane mesh contains 30 × 20 links.

In that case, in the y = 0 plane, following curves of the Figure 6 show maximum shear $\tau_1^{1,2}(x,0)$ and normal $\nu^{1,2}(x,0)$ stresses at the edge of the crack at the interface between the concrete and the asphalt layers where the load is at the left side of the crack (Guillo, 2004) .

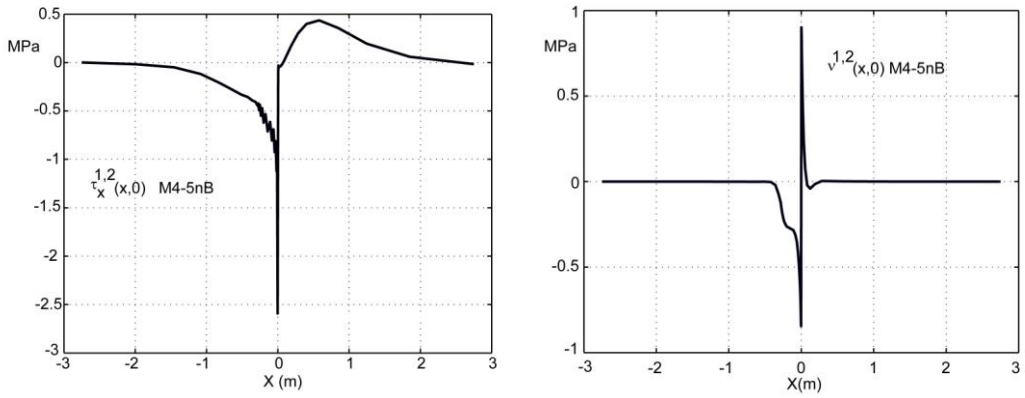

Figure 6. M4- 5nB stress fields between the cracked concrete layer and the asphalt layer

In this loading position at the crack edge, with the crack centered at zero on curves of the Figures 6, it can be observed that the pavement is loaded in mixed mode. These results needs to be examined in greater detail under actual experimental conditions (free edges along the y-axis; inclusion of thermal gradient effects in the thin bonded cement concrete layer and of the actual distribution of tire/pavement contact; comparison with instrumentation-based measurements; analysis of viscoelastic effects from asphalt material, etc.). Nevertheless, for the following purpose, it is interesting to notice that Figure 6 shows that the normal interface stress is highly negative underneath the load and remains significant in tension on the unloaded side.

5 FIELD OBSERVATIONS

Probably one of the most spectacular crack propagation cases might be corner crack damages that can be found on structures made with cemented concrete slabs. Here-under to illustrate, surface observations of distress from French yachting harbor pavement are given.

On pictures of the Figure 7, it shows a travelift crane that is used to take off boats from the sea to park them on a harbor. As it can be found in different constructor guides, these travelift are particularly heavy cranes (the load of the biggest is 300T) and move very slowly on four similar single or twin wheels. With boats, the loading is assumed to be worst.

Figure 7. Pictures of the heaviest travelift

On pictures of the Figure 8, one can see the small travelift used (Fig. 8a) and the pavement distress of cemented concrete slabs that are not loaded by the travelift wheels.

A: concrete slabs and the "Port Olona" Travelift

b: corner cracks in concrete slabs near loads

c: cracks in concrete slabs and bitumen structures

Figure 8. Example of pavement damages of a French harbor - Vendée, France

It can be observed that cracks are located especially on corner slabs of cemented concrete layer (Fig. 8b) although they exist in the whole bituminous structure under the wheel pass (Fig. 8c). One can supposed that loading slabs are made with special reinforced steel structure that can be true. Nevertheless, in a mechanical point of view it is interesting to correlate why cracks are located near corner slabs and high intensity value of normal interface stress that have been calculated as previously. On the corner of a slab, two free boundary conditions have to be written. That is supposed to be studied at LCPC with the help of the French cemetery industry to simulate crack corner distress of Ultra Thin White-Topping structures. In that study a tool for engineers on which it can be introduced different configuration of loads, shrinkage, debounding and even thermal gradient has to be done.

6 CONCLUSION AND PROSPECTS

To make a proper analysis of crack initiation and propagation in pavement structures, a simplified model (named the Multi-particle Model of Multi-layer Materials, M4) linked to the Boussinesq model for the soil has been developed (Tran, 2004) (Chabot et al., 2005). This approach has the advantage of reducing the real 3D problem to the determination of regular plane fields (x,y) per layer and interface. M4-5nB computations are in good accordance compared to 3D FEM results and need less time consuming. Several inelastic fields can be introduced as data for the modelling of shrinkage, thermal conditions and debounding effects. Near a pre-existing vertical crack through a layer, these special boundary conditions are proposed to be modeled to understand slab corner cracks phenomenon of Ultra Thin White-topping.

7 REFERENCES

Bodin, D. & Pijaudier-Cabot, G. & de La Roche, C. & Piau, J. M. & Chabot, A. 2004. Continuum Damage Approach to Asphalt Concrete Fatigue Modeling, *Journal of Engineering Mechanics (ASCE)* 130 (6): 700-708.

Carreira, R. P. & Caron, J. F. & Diaz Diaz, A. 2002. Model of multilayered materials for interface stresses estimation and validation by finite element calculations. *Mechanics of Material* 34: 217-230.

Caron, J. F. & Diaz Diaz, A. & Carreira, R. P. & Chabot, A. & Ehrlacher, A. 2006. Multi-particle modelling for the prediction of delamination in multi-layered materials, *Composites Sciences and Technology* 66 (6): 755-765.

Chabot, A. & Tran, Q. D. & Ehrlacher, A. 2005. A simplified modeling for cracked pavements - Modèle simplifié pour le calcul des chaussées, *Bulletin des Laboratoires des Ponts et chaussées* (258-259) : 105-120.

Chabot, A. & Tran, Q. D. & Pouteau B. 2004. Simplified modelling of a cracked composite pavement, *First International Elsevier Conference on Failure Analysis*, Lisbonne 12-14 juillet 2004.

Chabot, A. & Cantournet, S. & Ehrlacher, A. 2000. Analyse de taux de restitution d'énergie par un modèle simplifié pour un quadricouche en traction fissuré à l'interface entre 2 couches. In AMAC (ed.), *Comptes-rendus aux 12ème Journées Nationales sur les Composites (JNC12)*, ENS de Cachan 15-17 novembre 2000, 2 : 775-784.

Chabot, A. & Ehrlacher, A. 1998. Modèles Multiparticulaires des Matériaux Multicouches M4_5n et M4_(2n+1)M pour l'étude des effets de bord. In AMAC (ed.), *Comptes-rendus aux 11ème Journées Nationales sur les Composites (JNC11)*, Arcachon 18-20 nov 1998, **3 :** 1389-1397.

Chabot, A. 1997. *Analyse des efforts à l'interface entre les couches des matériaux composites à l'aide de modèles multiparticulaires de matériaux multicouches (M4)*. PhD thesis of the Ecole Nationale des Ponts et Chaussées.

Diaz Diaz, A. & Caron J. F. & Carreira, R. P. 2002. software application for evaluating interfacial stresses in inelastic symmetrical laminates with free edges, *Composites structures* 58: 195-208.

Duhamel, D. & Chabot, A. & Tamagny, P. & Harfouche, L. 2005. Viscoroute: Visco-elastic modeling for asphalt pavements - Viscoroute : Modélisation des chaussées bitumineuses. *Bulletin des Laboratoires des Ponts et chaussées* (258-259) : 89-103.

Guillo, C. 2004. *Validations par éléments finis d'un modèle simplifié pour l'étude de décollement à l'interface de multicouche de chaussée*. Rapport de stage de DESS de l'Université de Nantes.

Pouteau, B. & Chabot, A. & De Larrard, F. & Balay J. M. 2006. Mécanique des chaussées Béton sur grave-bitume, Etude de la tenue du collage entre béton et enrobé sur chaussée expérimentale (1re partie). *Revue Générale des Routes et des Aérodromes (RGRA)* (847) : 85- 90.

Pouteau, B. & Balay, J.-M. & Chabot A. & De Larrard F. 2004. Fatigue test and mechanical study of adhesion between concrete and asphalt. *9th International Symposium on Concrete Roads*, Istanbul 3-6 April 2004.

Pouteau, B. 2004. *Durabilité mécanique du collage blanc sur noir dans les chaussées*. PhD thesis of the Ecole Centrale de Nantes.

Romanoschi, S. A. & Li Y. 2002. Experimental characterization and modeling of fatigue and crack propagation in asphalt concrete layers. *BCRA'02 workshop on modelling of flex. Pav.*, Lisbonne.

Tran, Q. D. & Chabot, A. & Ehrlacher, A. & Tamagny, P., 2004. A simplified modelling for cracking in pavements. In RILEM Proceedings PRO 37, *Fifth International RILEM Conference Cracking in Pavements*, May 5-8 2004: 299-306.

Tran, Q. D. 2004. *Modèle simplifié pour les chaussées fissurées multicouches*. PhD thesis of the Ecole Nationale des Ponts et Chaussées.